

*Department of physics, École Normale Supérieure, Paris
Swiss Plasma Center, EPFL, Lausanne*

TRAPPED ELECTRON MODE
CHARACTERIZATION BY SHORT PULSE REFLECTOMETRY

Master Thesis 2024

Andrea Combette



Supervisors:

Dr. Oleg Krutkin

Pr. Jean François Allemand

Contents

<p>1 Theoretical Background</p> <ul style="list-style-type: none"> I Nuclear Fusion 2 1 Fusion Reaction 2 2 Tokamak confinement 2 <p>II Transports in Tokamak 3</p> <ul style="list-style-type: none"> 1 Trapped particles and drifts 3 a) Trapped particles 3 b) Drift waves 3 2 Radial Transport 4 <p>III Wave propagation in plasma 4</p> <ul style="list-style-type: none"> 1 Plasma as a medium 4 2 Wave equation 5 <p>IV CUWA code overview 5</p> <p>V Linear Regime Study 6</p> <ul style="list-style-type: none"> 1 Perturbed Density Profile . 6 a) General perturbation profile 6 b) Step-like perturbation 6 b).1 Model 6 b).2 Results 7 <p>2 1 dimensinal Model</p> <ul style="list-style-type: none"> I Reliable metrics 8 II Machine Learning Model 8 1 structure 8 III Input Data 9 IV Datasets building 9 	<p style="text-align: center;">CONTENTS</p> <hr/> <p>V Results 10</p> <p>3 2 dimensinal Model</p> <ul style="list-style-type: none"> I Pulse shape Study 10 1 Relative Study of Pulse Shape 10 2 Statistical Study of Pulse Shape 11 3 Gaussian fitting of the pulse 12 4 Detection of scattered pulse 12 <p>II Datasets building 12</p> <ul style="list-style-type: none"> 1 Gaussian spectrum of the turbulences 12 2 Power Spectrum of the turbulences 12 a) CORrelation length depen- dancy study 13 3 data scanning 14 <p>III Results 14</p> <ul style="list-style-type: none"> 1 Global performance 14 2 Comparison of the prediction with other models 15 a) Mean delay study 15 b) Amplitude pre- diction study 16 c) standard devioda- tion of delay 16 3 Results on experimental datasets 16 <p>4 Conclusion and Discussion</p> <p>5 ACKNOWLEDGMENTS</p>
--	---

ABSTRACT

ONE of the common goals in experimental magnetically confined fusion research is characterization of the plasma turbulence. To that end, TCV tokamak features a novel short-pulse reflectometry (SPR) diagnostic, which can potentially be utilized to measure properties of the turbulence. It is essentially a radar system, where the plasma is probed by a short (under ns) microwave pulse in the presence of the cut-off (reflection) area from which the pulse reflects back into the probing antenna. The position of the cut-off for a particular probing frequency (50-75 GHz) range is determined by the plasma electron density. Thus, by measuring the delay between probing and reflected pulse corresponding to different probing frequencies, the information about the electron density profile is inferred including its turbulent perturbations. Unfortunately, the complex interaction of microwaves with magnetized plasma makes it difficult to establish the connection between SPR measurements and properties of the turbulence. Numerical modeling utilizing the synthetic diagnostic approach was carried out to establish this connection for the case of low turbulence amplitudes (linear regime). However, the case of large turbulence amplitudes (nonlinear regime) is yet to be explored. Within the project a systematic analysis of the SPR diagnostic in the nonlinear regime will be carried out. The numerical finite difference code CUWA, which solves the wave equation for a given plasma density, magnetic field and provides synthetic reflected pulse will be utilized. The main goal of the project is identifying markers that can be used to determine if the diagnostic is operating in the nonlinear regime and assessing the possibility of determining the turbulence parameters regardless.

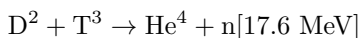
CHAPTER 1

Theoretical Background

I Nuclear Fusion

1 Fusion Reaction

THE nuclear fusion reaction is the process by which two atomic nuclei combine to form a heavier nucleus. It is accompanied by the release or absorption of energy depending on the masses of the nuclei involved. Indeed, the lighter are nuclei, the more energy is released due to the overcoming short-range nuclear force for light nuclei. However, to overcome the Coulomb barrier the reactant must be sufficiently close for a long enough time to allow the quantum tunnel effect between both particles. To do so, we must heat up the reactant to huge temperatures such that these latter are ionizing and turning into plasma. We found that the probability of collision (cross section) is the best for the Deuterium-Tritium mix.



2 Tokamak confinement

The key component of the fusion process is how long we can confine the plasma. This confinement can be of several kinds. One of the most promising and old, is the Tokamak vessel, which uses magnetic confinement to keep the plasma in a toroidal shape. The plasma is heated up to several million degrees, and the fusion reaction can be sustained. The energy released by the fusion reaction is used to heat up the plasma, and to sustain the reaction. The energy balance is given by the Lawson criterion, which is a measure of the energy confinement time over the energy loss time. The energy confinement time is given by the plasma density, temperature and the energy loss time is given by the plasma losses.

$$n\tau E \geq 1.5 \cdot 10^{20} \frac{\text{s}}{\text{m}^3}$$

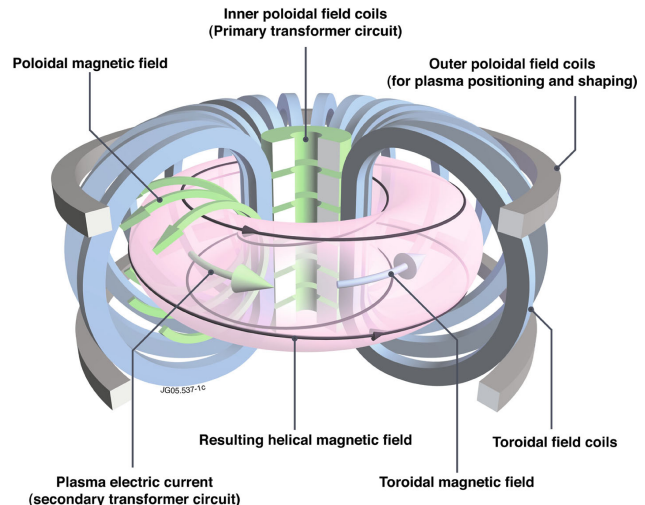


Figure 1.1: simplification of Tokamak device, the toroidal magnetic field is generated by the coils, and the poloidal magnetic field is generated by the plasma current and the poloidal field coils. The plasma is heated up by several device, and the fusion reaction can be sustained.

This confinement is realized by applying a strong magnetic field in the toroidal direction. The magnetic field is generated by a set of coils, which are arranged in a toroidal shape, and the plasma is heated by various method [1]. The neoclassical geometries at stake in the tokamak leads to several physics phenomena such as charge separation in the tokamak, drifts cinematic and turbulences. The curvature and the gradient of magnetic field [2] imposed by the geometry leads to $E \times B$ drift. Which impose to the tokamak a poloidal magnetic field component to counter this effect. This twist in the field line is called the safety factor and is defined as :

$$q(\Psi) = \frac{1}{2\pi} \frac{\delta\chi(\Psi)}{\delta\Psi} \approx \frac{B_{tor}r}{B_{pol}R},$$

With χ the toroidal magnetic flux. This safety factor is one of the most important measures in tokamak since the induced magnetic properties on the rational magnetic surface ¹ are of paramount importance for the confinement of the plasma. Indeed, we can define the shear stress as $\hat{s} = \frac{r}{q} \frac{dq}{dr}$, which measures how much the magnetic field line are twisted along the small radius

¹Only rational value of the safety factor allows periodic field line



of the tokamak. This shear explains why the turbulences grow on rational surfaces (no Landau Damping $k \cdot B = 0$, [3]), and how they are damped into bigger scale flow (zonal flow) see [4]. Indeed, the consideration of the magnetic surfaces is also at the foreground for solving Ballooning equations in toroidal geometry, since it will drive the definition of the toroidal functions of Ballooning modes, every discussed instabilities can be expressed using a toroidal geometry in the Ballooning space [5, 6]. In addition to that the safety factor allows to have an insight of the strength of the toroidal current, which follows the q -profile (max in the center), this explains why the toroidal velocity of particle is lower on the edge than in the center, which allows some particle to be trapped in banana orbits.

II Transports in Tokamak

Anomalous transport is a crucial subject in tokamak research, indeed it causes a huge drop of the energy confinement through a enhanced particle radial flux. Here we will study micro-instabilities, i.e small scale turbulences (gyro-bohm scaling [4]), whose radial transport is really high and largely controlled by low frequency modes [6]. For these type of instabilities, the study is based on Kinetic Vlasov theory. Several types of micro-instabilities exists from **TEM** to **ITG** and **ETG** instabilities. These instabilities cause a transport of energy from the core of the plasma to the edge, where it can be evacuated, the largest transport in the TCV is due to the unstable **TEM** mode [7, 8]. This mode is the results of the resonant interaction between trapped electron and Drift Wave (DW), it can be collisionless or dissipative, basically the trapped electron are transferring energy to the growing wave.

1 Trapped particles and drifts

There are two type of kinetic for electrons in the tokamak : run-away or passing and trapped electrons. Majority of the electrons are passing since to be trapped electrons must verify : $v_{\parallel} \ll v_{th}$ [9][10]. However trapped electrons present a transit time much larger than passing one, this leads to greater interaction with the DW. These different of behavior regarding the DW leads to small scale instabilities.

a) Trapped particles

For a colisionless plasma $\nu \ll w$, with ν the colision frequency and w the frequency of the considered wave, the main radial transport is caused by particle with low parallel velocity. Indeed, when the toroidal component of the magnetic field is much larger than the poloidal component, $|B_{\Phi}| \gg |B_{pol}|$ we have the simple B relation for a torus

$$B \propto \frac{1}{R - R_0},$$

then in the (r, θ, z) coordinates we have :

$$B = B_0 \left[1 - \frac{r}{R_0} \cos(\theta) \right]$$

Hence, taking into account the toroidal drift we can derive the following equations using the guiding center equations [9]:

$$\frac{d}{dt} \left(r + \frac{m}{qB_p} v_{\parallel} \right) = 0, \quad r - r_0 = -\frac{m}{qB_p} v_{\parallel}$$

r_0 indicates the position of the turning point where the mirror effect occurs [11]. To be trapped the particle velocity should verify $v_{\parallel} \ll v_{\perp}$ more precisely from a simple energetic approach [8]

$$0 \leq v_{\parallel} \leq \sqrt{2\epsilon}v_{\perp}.$$

This partially explains why the velocity distribution of the electron [8, 10]is modified from a Boltzmann distribution to a more complex one, leading in a drop of conductivity (Spitzer condicivity). This also explain why the **TEM** dissipative and colisionless are highly locallized in the trapped electron region. The banana shape formed has then the following width :

$$\Delta r = \frac{m}{qB_p} v_{\parallel}$$

This banana shape can be interpreted as a simple Lorentz force acting on the particle animated by a sufficiently high vertical drift motion.

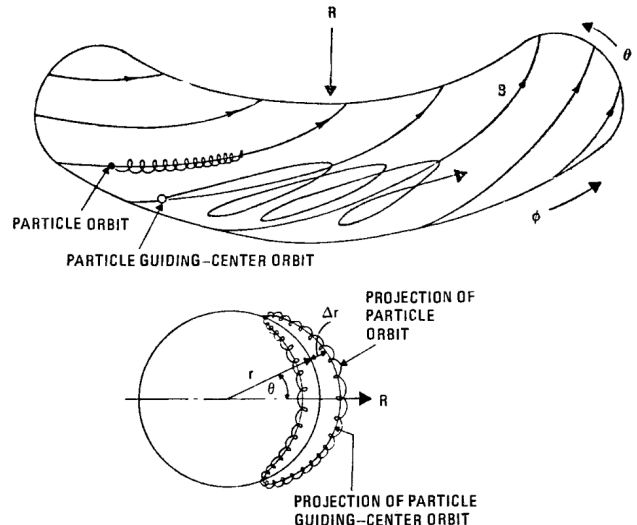


Figure 1.2: Trapped particle motion in the tokamak, the banana shape is due to the toroidal magnetic field, the particle is trapped in the magnetic well, and can interact with the DW. the second figure shows a cross section of the torus where we project the one banana orbit of the particle. From [9, 10]. Hence, if a wave is resonating with the particle, with a lower frequency than the transit time of the particle, the particle can exchange energy with the wave in a quasi-adiabatic way. (see after)

b) Drift waves

Electron DW instabilities that are at stakes here are governed by the famous **Hasegawa-Wakatani** [12, 13] equation due to non-adiabatic response of the electrons (the equilibrium is not reached after each oscillation of the wave) derived from a simple version of the drift kinetic equation from Vlasov theory. Hence, let's remind the general form of the general form of the H-W equation :

$$\begin{cases} \rho_s^2 \frac{d}{dt} \nabla_{\perp}^2 \Phi = D_{\parallel} \nabla_{\parallel}^2 (\tilde{\Phi} - \frac{T\tilde{n}}{|e|n_0}) \\ \frac{1}{n_0} \frac{d}{dt} \tilde{n} + \frac{v_r}{n_0} \partial_r n_0 = D_{\parallel} \nabla_{\parallel}^2 (\tilde{\Phi} - \frac{T\tilde{n}}{|e|n_0}) \end{cases} \quad . \quad (1.1)$$



With ρ_s the ion sound radius, D_{\parallel}^2 the parallel diffusion coefficient, Φ the electrostatic potential, \tilde{n} the density perturbation, v_r the radial velocity, n_0 the equilibrium density, T the electronic temperature, e the electron charge.

In the adiabatic limit [14], i.e when the particles diffuse faster than the wave, we can assume a simple a Boltzmann distribution of electrons with a small perturbation :

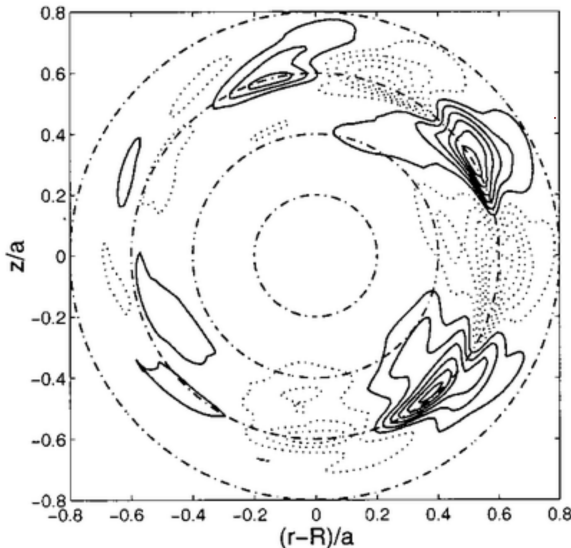
$$\frac{\tilde{n}}{n} \approx \frac{|e|}{T} \tilde{\Phi} + \tilde{h}$$

this finally leads to the **Hasegawa-Mima** [15] equation under the assumption : $v_{thi} < \frac{w}{k_{\parallel}} \ll v_{the}$.

$$\begin{cases} \rho_s^2 \frac{d}{dt} \nabla_{\perp}^2 \tilde{\Phi} \approx \frac{1}{n_0} \left(\frac{d\tilde{n}}{dt} + v_r \partial_r n_0 \right) \\ \partial_t \frac{|e|\tilde{\Phi}}{T} + \partial_r \tilde{h} - \rho_s^2 \frac{d}{dt} \nabla_{\perp}^2 P \tilde{h} + v^* \partial_y \frac{|e|\tilde{\Phi}}{T} = 0 \end{cases} \quad (1.2)$$

With $v_* = \rho_s c_s / L_n$ and L_n the gradient scale of the equilibrium density $-\partial_r n_0 / n_0$. This leads to the following dispersion relation for the drift waves with w_r the real frequency of the wave and γ the growth rate (the imaginary part of the frequency) :

$$\omega_r = \frac{w_*}{1 + k_{\perp}^2 \rho_s^2}, \quad \frac{\gamma}{w_r} = \pi \frac{w_r - w_*}{k_{\parallel} v_{e,th}}$$



We can denote $\frac{w-w_*}{k_{\perp}^2 v_{e,th}}$ the non-Boltzmann factor for electron DW. The reader will note that this study is independant of trapped electron, this is why in order of magnitude the growth rate is quite low, however when we increase the transit time of electron (by trapping), we can show [Sazn_diego], that the non-Boltzmann factor is increasing, leading to a higher growth rate, notably because of the introduction of $w_{D,e}$ the electron curvature drift frequency. Indeed, for colisionless trapped electron mode the non-Boltzmann factor is given by : $\frac{w-w_*}{w_{e,D}} e^{-R/L_n} \sqrt{\frac{R}{L_n}}$ which is definitively larger than the electron DW non-Boltzmann correction factor. leading to the following growth rate :

$$\frac{\gamma}{w_r} = i\pi \frac{w-w_*}{w_{e,D}} e^{-R/L_n} \sqrt{\frac{R}{L_n}},$$

explaining why **CTEM** are much more unstable than classical electron DW. Explaining also why the main instabilities are located in the banana region where the coherence time of the electrons are much more larger, same conclusions can be driven from the Dissipative Trapped electron mode [14]. This instabilities leads to inverse cascade of energy (*Kolmogorov*), contributing to highly non linear interaction with mesoscale structures (zonal flow) [6, 7, 16].

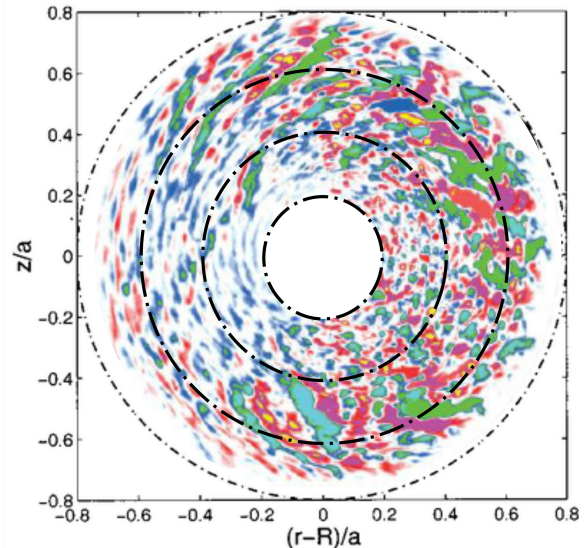


Figure 1.3: Cross section view of tokamak with negative shear flow - On the left we have the fourier Ballooning mode $n = 6$, characteristic from the TEM mode, it presents this characteristic tilting of the wave vector k_{\perp} , and a radial translational symmetry. On the right we have a simulated TEM mode, with the same shape structure characteristics, we will note the presence of multiple modes, teared and more tilted by the zonal flow, explained by the non linear interaction between these two types of flow, reproduced from [17, 18]

2 Radial Transport

These micro-instabilities are one of the best candidates to explain high radial transport, indeed as we saw previously the resonating trapped electron allows a high fluctuation in the density field and in the magnetic pressure. Indeed we can show that the radial particle flow does not vanishe (as normal), in this case with a high contributio of the resonant trapped electron to the mean transport [16]. This radial dependency is the only density dependency retained for the following

part.

III Wave propagation in plasma

1 Plasma as a medium

To study the density profile, many diagnostics methods exists ,like Doppler Reflectometry, RCDR, Short pulse reflectometry ... The study here will be based

²the parallel diffusion coefficient provides insights of the electrons-ions collision frequency $D_{\parallel} = \frac{v_{the}^2}{\nu_{ei}}$



on the Short Pulse Reflectometry (**SPR**), this method consists in probing the magnetized plasma with a short gaussian Pulse (<ns) microwaves operating in the time domain at a fixed frequency under normal incidence with respect to the cut-off surface and the variation of the delay of the reflected pulses. The probing signal, is sensitive to density variation since it will change the cut-off position, this is why it can be used to have deeper insights of the turbulences characteristics

2 Wave equation

Assuming a monochromatic electromagnetic-wave and using the Maxwell equations, we can derive the local complex dielectric tensor, and the considered wave wave equation :

$$\left. \begin{aligned} \nabla^2 E - \vec{\nabla} \nabla \cdot E &= -\frac{\omega^2}{c^2} \hat{\epsilon} E \\ \hat{\epsilon}_{ik} &= \delta_{ik} - \frac{4\pi i}{\omega} \sigma_{ik} \end{aligned} \right\} \quad (1.3)$$

with σ_{ik} the conductivity tensor. To establish this equation multiple assumption have been made, linear Ohm's law is applicable, cold plasma (cite), neglect chaotic motion of the particles, which implies neglecting the kinetic effect. To simplify the problem we will assume the plasma to be stationnary and neglect all kinds of damping. Then in a carthesian coordinates system with z axis driven by a constant magnetic field, $\vec{B} = B_0 \vec{e}_z$, we can derive the following dielectric tensor [**Thomas H.Stix**]

$$\hat{\epsilon} = \begin{pmatrix} \epsilon & ig & 0 \\ -ig & \epsilon & 0 \\ 0 & 0 & \eta \end{pmatrix}$$

With : $\epsilon = 1 - \frac{\omega_{pe}^2}{\omega^2 - w_{ce}^2}$, $g = \frac{w_{ce} w_{pe}^2}{w(w^2 9 W_{ce}^2)} - \frac{w_{ci} w_{pi}^2}{w(w^2 9 W_{ci}^2)}$;
 $\eta = 1 - \frac{w_{pe}^2}{w^2} - \frac{w_{pi}^2}{w^2}$; $w_{pi} = \sqrt{\frac{4\pi n e^2}{m_i}}$; $w_{ci} = \frac{eH}{m_i c}$

w_{pi} stands for the electron or plasma frequency and w_{ci} is the cyclotron frequency for the i species. We will consider the electron component preponderant in the next study since we are dealing with microwave frequency. The wave equation can be simplified to the following :

$$\left. \begin{aligned} (S_{yz} - \epsilon)E_x - igE_y - \Pi_{xy}E_z &= 0 \\ (S_{zx} - \epsilon)E_x + igE_x - \Pi_{yz}E_z &= 0 \\ (S_{xy} - \eta)E_z - \Pi_{xz}E_x - \Pi_{yz}E_y &= 0 \end{aligned} \right\} \quad (1.4)$$

Defining : $S_{ij} = N_i^2 + N_j^2$; $\Pi_{ij} = N_i N_j$; $N_i = \frac{k_i w}{c}$
For the **SPR** study the wave is perpendicular to the external magnetic field, hence we can simplify the system to the following :

$$\left. \begin{aligned} (N_y^2 - \epsilon)E_x - igE_y &= 0 \\ (N_x^2 - \epsilon)E_y + igE_x &= 0 \\ (S_{xy} - \eta)E_z &= 0 \end{aligned} \right\} \quad (1.5)$$

Which leads to two different types of solution respectively the ordinary mode (\mathcal{O}) and the extraordinary mode (\mathcal{X}).

\mathcal{O}	\mathcal{X}
$S_{xy} - \eta = 0$	$(N_y^2 - \epsilon)E_x - igE_y = 0$
$E_y = 0$	$(N_x^2 - \epsilon)E_y + igE_x = 0$
$E_x = 0$	$E_z = 0$

The \mathcal{O} mode corresponds to the mode with electric field parallel to the external magnetic field, hence the propagation does not depend on this latter but only on the density profile. The \mathcal{X} mode is the mThisode with electric field perpendicular to the external magnetic field, hence the propagation depends on the magnetic field and the density profile. The dispersion relation of the wave can be derived locally from the wave equation, and we can obtain :

$$k^2 = \frac{w^2}{c^2} \eta \approx \frac{w^2}{c^2} \left(1 - \frac{n}{n_c} \right); \quad n_c = \frac{m_e w}{4\pi e^2} \quad (1.6)$$

Here we can see that the wave number vanish at $n = n_c$, this is the cut-off layer where the wave is reflected. The k-spectrum of the \mathcal{X} is much more complicated and include plasma resonances where thermal effects must be taken into account. For this study we will limit ourself to the \mathcal{O} mode. Then from solving the Helmotz equation (local dependancy of the wave number)

$$\frac{\partial^2 E_z}{\partial x^2} + k(x)E_z = 0$$

and appying the **WKB** approximation (slow variation of the plasma parameters), i.e assuming a a solution of the form $E_z = A(x) \exp(i\Phi(x))$, with A varying slowly and Φ varying quickly, we can derive the following expression for the Electric field:

$$E_z(x) = \frac{E_z}{\sqrt{\frac{c}{w} k(x)}} \exp \left(i \int_0^x k(x') dx' \right)$$

The WKB approximation will be used in the one dimensional approach (see Chapter 2), and in the **CUWA** code for computing the ray tracing in order to adjust the size of computation Yee cells [19] and the computation domain.

IV CUWA code overiview

The CUWA code is a **GPU** based computations scheme with a Python-CUDA frameworks, using finite difference scheme for spatical dependancy applied to the three different fields : E, B, J and the well-known leap-frog time stepping. It is used to simulate the propagation of electromagnetic wave inside a "cold plasma". The sqaial finite difference scheme is based on the FDTD Yee's method [**Yee**], with slight modifications. It solves the discrete version of the Maxwell's equations with a cold Plasma current Response \mathbf{J} :

$$\left\{ \begin{array}{l} \frac{\partial}{\partial t} \mathbf{B} = -\nabla \times \mathbf{E} \\ \frac{\partial}{\partial t} \mathbf{E} = c^2 \nabla \times \mathbf{B} - \frac{\mathbf{J}}{\epsilon_0} \\ \frac{d}{dt} \mathbf{J} \nu \mathbf{J} = \epsilon_0 w_p^2 \mathbf{E} - \mathbf{J} \times \mathbf{w}_c \end{array} \right. \quad (1.7)$$

with w_p the electron plasma frequency, ν the electro collision frequency and w_c the electron cyclotron frequency. To limit the computational cost, the computation domain is amended with a convolutional perfectly matched layer (**PML**) to ensuring any reflected singals are small (well used in open boundaries system). It can be viwed as a sponge layer for electromagnetic wave.

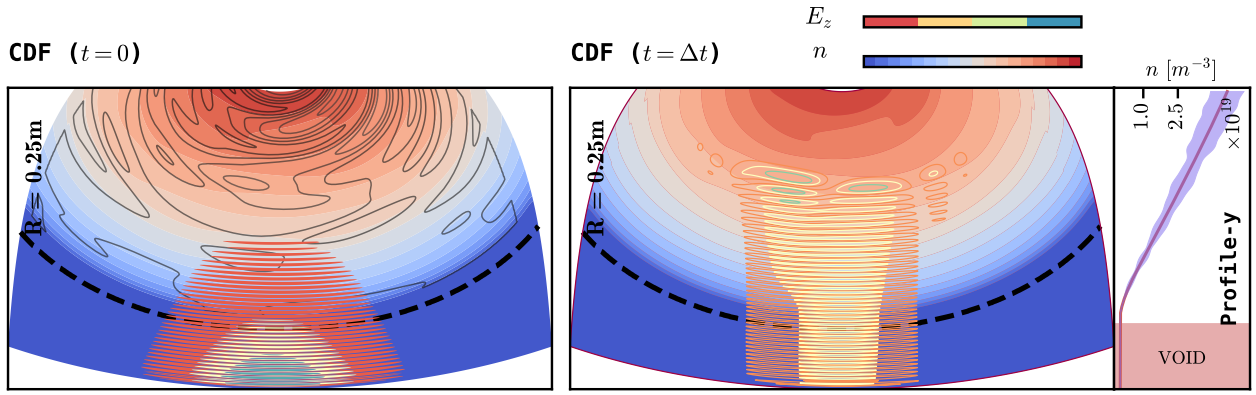


Figure 1.4: SPR setup using the *O.Krutkin and A.combette LEONARDO simulations from the CUWA code*, the probing wave is sent to the plasma, and the reflected wave from the cut-off is measured, the delay between the two waves is a measure of the plasma density profile, in addition to the pulse shape that has been altered by the turbulences (eq). Here we plot the contours of the density profile, with cold density perturbations (black contour lines on the left plot), the probing wave is reflected by the cut-off layer (initial probing wave on the left and after a $\Delta t \approx 10\text{ns}$ we got the reflected scattered wave on the right). The third plot on the right shows the density profile width its perturbations (filled), a liner density profile

$$n(x, y) = \frac{x}{L} (n_c + \delta n(x, y)).$$

as been chosen according to (cite). Note that this linear correction made on the amplitude of the turbulence fields, follows from the non-adiabatic perturbations [16] AND NUMERICAL INSTABILITY, and his more relevant than a simple constant amplitude turbulence field. The curvature of the grid has been set to the $R = 0.25\text{m}$ to mimic the TCV geometry.

V Linear Regime Study

The goal of this study is to find a way to link the plasma density perturbations to the reflected pulse characteristics. First we will study a simple 1 dimensional model proposed by (*Oleg Krutkin*) applied in a given range of turbulence amplitude and size and then we will extend this study to a more general 2D model using the **CUWA** code. Assuming a simple plasma density profile $n(x)$, we can study the wave propagation in the plasma. The goal of this approach is to find a way to link the plasma density perturbations to the reflected pulse delay. To retrieve some information about the pulse delay we will use a statistical approach to get rid of the randomness implied by the perturbations considerations. The delay of the probing wave is given by the following formula :

$$\tau_c = 2 \int_0^L \frac{dx}{v_g}$$

Where v_g is the group velocity of the wave, L is the position of the cut-off. From the simple assumption $\langle \delta n \rangle = 0$ for an Ordinary mode the v_g expression obtained [] can be used to expand the integral to the following :

$$\frac{2}{c} \int_0^L \frac{dx}{\sqrt{1 - \frac{x}{L} - \frac{\delta n}{n_c}}}$$

The main contribution of this integral comes from the vicinity of the cut-off layer, Where the group velocity is the smallest. We can discuss the relevance of this expansion this the main contribution of the integral comes from the cut-off region where the WKB approximation cannot be applied.

1 Perturbed Density Profile

a) General perturbation profile

First let's consider to simplify a gaussian perturbation density profile (we will see later that the spectrum of the vector number is not a gaussian but a non trivial power spectrum due to the two type of energy cascade). From this, the considered integral can be written in the following way :

$$\tau_d = \frac{2}{c} \int_0^L \frac{dx}{\sqrt{1 - \frac{x}{L} - \frac{\delta n_0 \exp\left(-\frac{(x-L)^2}{8l_{cx}^2}\right)}{n_c}}}$$

With l_{cx} the correlation length of the turbulence field and δn_0 the amplitude of the turbulence field. This integral is not trivial to solve in from an analytical way, which is necessary to exhibit the possible statistical features of the dealay. This is why we can suggest developing a first order perturbation profile which leads to step like perturbations.

b) Step-like perturbation

b).1 Model With a step-size perturbation characterized by l_{cx} length. This allows to get an analytical expression of the integral for different density profile. However, to get this simplification, we need to assume that the perturbation is small enough such that the WKB approximation can be applied. This is the case for the linear regime, where the perturbation is small enough such that the cut-off layer is not too much perturbed (i.e $\delta_x \ll l_{cx}$). In the case of a large perturbation, an other step perturbation localized far from the cut-off layer can be used to get the same result,



which breaks the main assumption of this approach (see fig.1). It's relatively trivial to obtain the following expression for the delay [cite Krutkin] :

$$\tau_d = \frac{4L}{c} - \frac{2L}{c} \sqrt{\frac{L}{l_{cx}} \frac{\delta n}{n_c}}$$

The statistical approach is to consider the perturbation as a random variable, and to compute the statistical properties of delay of the probing wave. This approach is relevant for the linear regime, where the perturbation is small enough such that the cut-off layer is not too much perturbed (i.e $\delta_x \ll l_{cx}$). For example

we can compute the standard deviation of the delay depending on the standard deviation of perturbations. This gives us the following at first order :

$$\sigma_{\tau_d} \approx \frac{2L}{c} \sqrt{\frac{L}{l_{cx}} \frac{\sigma_{\delta n}}{n_c}}$$

To test this assumption we can compare the analytical expression with the numerical integration of the wave equation, for numerous gaussian perturbations with characteristics length l_{cx} and various amplitudes δn , depicted in the figure 1.6.

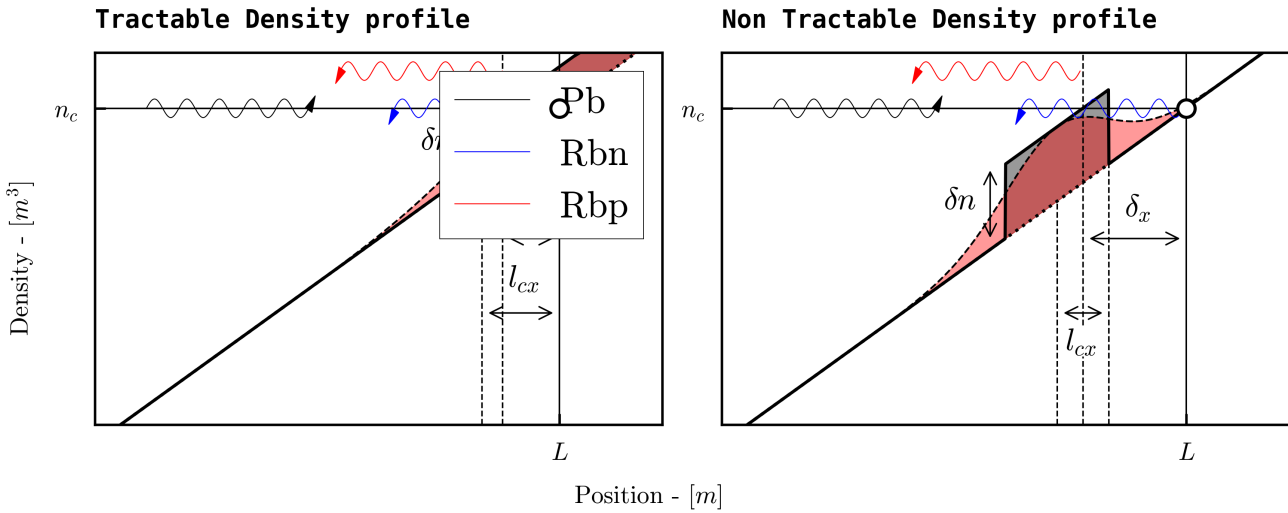


Figure 1.5: Here we plot the density profile of the plasma for different perturbation amplitude, in grey the step-like model perturbation and in coral the gaussian one. For large value density perturbation, the model leads to a contradiction with its assumption $\delta x < l_{cx}$ or $\delta n < n_c \frac{l_{cx}}{L}$, given by a small cut-off layer shift. The blue Pb wave is the probing wave, red Rbp wave is the reflected one and blue Rbn wave is the normal reflected wave, in absence of perturbation.

One sample of density fluctuation is produced using the following formula, to match a supposed gaussian spectra of instabilities :

$$\delta n(k_x) = \delta n_0 \exp \left(-\frac{(k l_{cx})^2}{8} + i \Phi(k) \right)$$

with $\Phi(k)$ a random phase, k the radial wavenumber of the density perturbation and δn_0 the amplitude of the perturbation, this amplitude can be taken constant or dependant of the radial position according to the kind of profile we use. Then we inverse fourier transform this density perturbation to get the density profile in the real space. Finally, for each sample, the delay is then numerically integrated from the formula [cite delay], using simple trapezoidal integration.

b.)2 Results The results are shown in the figure 1.6, the simulated deviation of delay (black cross) was computed on 10000 samples to ensure statistical stability, with a 50 GHz probing wave and a $2L$ integration domain, allowing us to take into account negative perturbation near the cut-off, indeed if there is multiples ones near the standard cut-off it might strongly shift this latter. The plain black line is the 1st order approximation of the formula [eq] and the dashed one as the

third order approximation of the second formula. The numerically integrated delay, which stands as reference is in black cross. The second order analytical formula presents a characteristic drop-off (as the simulated delay) after reaching a critical value amplitude. This critical value can be defined by two way [PUT, 20] and fix the threshold of what we could later the **Non linear** regime. Which can suggest than expanding further the σ_{τ_d} which leads to a better handling of non-linear domain. However, in both cases some discrepancies are observed for large perturbations in Non Linear regime, but the analytical expression seems to be a good approximation for small perturbations, except for really tiny one [cite]. However, one have to introduce a correction factor to the analytical expression to get a better agreement with the numerical integration. This l_{cx} dependant factor is given has not been studied yet but it highlights the limitations of current step driven 1D model ³. The non linear regime is strongly related to scattering effect, which are not taken into account in this approach. In addition to that, generally the density corrugation reaches a level of 100 % of the density value near the cut-off [7], especially since the adiabatic and non adiabatic component of the electron response have the same potential dependency [16]. Hence the non-linear regime is non

³The integration of the gaussian integral was also tackled, with a second order bell-approximation, leading to logarithmic dependancies over the plasma parameters, however the formula was too complicated to exhibits the statistical properties of the delay refers to appendix



negligible and of necessity to find a sufficiently precise model to evaluate turbulences amplitudes in **NL** regime.

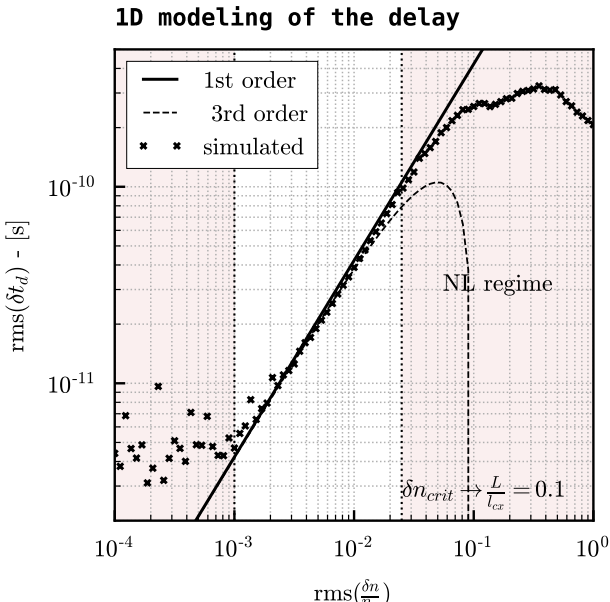


Figure 1.6: 1 dimensional predicted amplitude of the analytical 1st and 2nd order step driven model, compared to the simulated 1 dimensional delay see eq :1.6, a constant δn_0 has been used for the density profile

Hence, the first arised issue is to find a good parametrization of the model (i.e find the best statiscial metrics) to predict the amplitude of the turbulence. This study will be done using several profile of density perturbations amplitudes δn_0 , to see if the model we build is sufficiently robust to adapt.

CHAPTER 2

1 dimensinal Model

The first model we tried to build relies simply on the 1 dimensional integration of the delay. Hence, for this simple model wa can only rely on the pulse delay statistical properties. Several options had been tested from the study of the quantile repartition of the delay, its histogram , and several statisctial properties of this latter. Then the study consists in a simple multidimensional regression problems where we will try to estimate the amplitude of the perturbation and the non-perturbed delay of the probing wave (i.e without the turbulenecs fields) and this for several density profile. In order to tackle this problem we used a stacked regressor, combined with a multi-output one.

I Reliable metrics

To train our Machine Learning model, we need some clear data, with the best input as possible. So first let's try to understand the characteric of the delay. To have a general overview of the influence of the turbulence amplitude δn_0 on the delay characteric, the best way is to study the distribution of this latter in function of the amplitude, this is done in the following plot.

Normalized Delay Violins

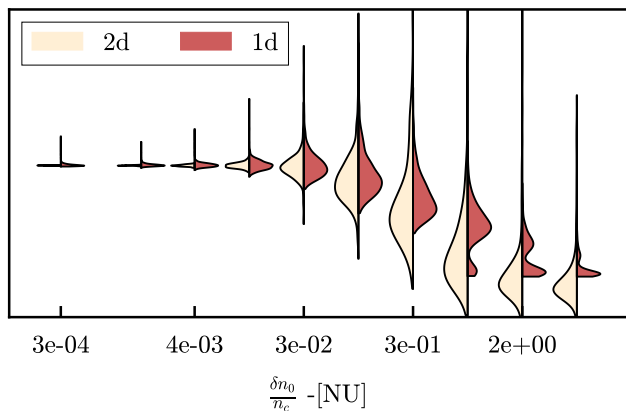


Figure 2.1: Violins plot of the delay distribution over δn_0 . Here we choose for a simple first approach a simple linear profile with δn_0 independant of the radial position. The left side of each violins stands for the 2d distribution of the delay for comparison.

The first thing that we can unearth is that the delay distribution is well disturbed by an amplitude increasing, the mean delay decrease (which is quite obvious see ??), the standard deviation of the delay increases and when we reached the non-linear regime it starts decreasing. The distribution seems also to be more more skewed until we reach the non linear regime, this indicates that the study of the momemt of the delay distribution can also be a good way to predict the amplitude level. The two-simulation sets present quite the same behaviour, however at high amplitude the 1d simulation set present some discrepancies with the 2d one, indeed the distribution is more eratic, this can question the good convergence of the 1D integration (see : 1.6). In addition to that, we can highlight that the critical density unearthed by this plot is the first critical density (CITE), which is of great importance to buiild a qualitiative dataset. Still, the delay study should lead to a good estimation for both simulation sets, even without pulse shapes study allow with the 2D model. Hence, let's see if the delay study can be a sufficient estimator for amplitude level prediction in both dimensionalities.

II Machine Learning Model

The machine Learning model will learn to predict the amplitude δn_0 and the default delay without amplitude τ_0 , with one one dimensional training set, and will be test on a one dimensional and a two dimensional testing set.

1 structure

The regression model we used is a stacked-multioutput regressor

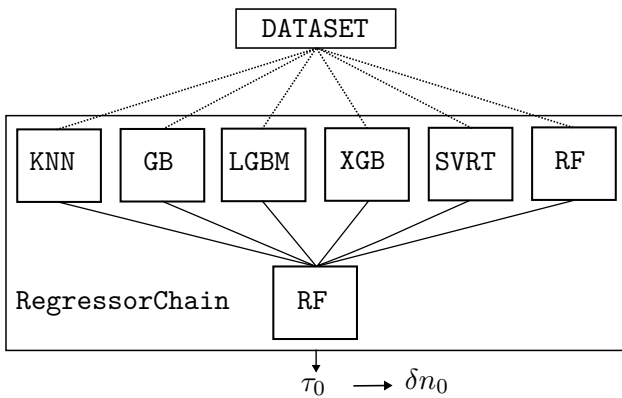


Figure 2.2: stacked Regressor structure with global regressor chain, the internal struture of the multiple regressors are not detailed for simplicity, but each one is a complex model with specific advantage and limitations, we tested each model on several datasets, and the combination of them is a key in the performance of our prediction specially in limit cases, with high or low turbulences amplitude.

Our model combines the following models : K-neighbors (KNN), Random-forest (RF), 3 different Gradient-Boosting (GB, LGBM, XGB), and support vector (SVR) , regressors, it is made to be as general and versatile as possible. Then the 6 models are trained in parallel on the same training datasets, in series with a decision regression model which is in our case a final RF layer trained on the outputs of previous layers. Normally the Gradient-Boosting models can not handle multi-output regression, this is why we used a multi-output **RegressorChain**. This model train the model to predict the the first entry and then to predict the second given the first prediction, this allows to incorporate a dependancy between the different outputs, which should not be the case here, so normally a simple **MultiOutputRegressor** should be sufficient. Let's note that the score of the final model cannot be less than the score of the best model. The following table described the hyperparameters used for the stacked model.

Model	Hyperparameters
KNN	n_neighbors : 20
RF	n_estimators : 300 max_depth : 40
GB	n_estimators : 200 lr : 0.005
LGBM	n_estimators : 200 lr : 0.005
XGB	n_estimators : 200 lr : 0.005
SVR	kernel : 'rbf' C : 1 epsilon : 0.01

Table 2.1: Main Hyperparameters used for the stacked model, the error use is not detailed as long as the performance tweaks

III Input Data

IV Datasets building

For the 1D based trained model, we can only use the delay distribution as input variables. We tried several moment of the distribution as input (mean, variance, skewness...), combined with the discretized delay distribution. We tested two types of discretization, the binned distribution and the quantile distribution. However, we reached better results with the quantile study of the distribution, coupled with the moments as input. This allows the model to have a direct connection between the output τ_0 and the quantilized distribution. We use in both case 30 quantiles to discretized the distribution. The 1D simulations set is then processed, splitted in a training and a testing set (80/20 ratio) and finally standardized, the amplitude parameter was used with its logarithmic value because it was find to be more efficient. Hence we arrived to a final input shape of 33 features and ~ 3000 samples, including the L, l_{cx} paraemters in the input data. For the 1D simulation, we introduced a random shift in the delay distribution for each sample, indeed if we dont do that the model will learn τ_0 value from the highly coerrelated parameter L (originally L is linear with τ_0) which might be not the case in experimental data, where L can stand for the gradient scale at the cut-off [7]. For this study we used several density profiles to see if they have a real impact on the learning process of the model. For the 1D simulations the dependancy over y is dropped. For the linear background profile, the global density profile will be the following :

$$n(x, y) = n_c \frac{x}{L} + \delta n_0(x) \delta n(x, y).$$

With δn the 2D gaussian turbulence profile For the quadratic background profile L , stands for the gradient scale at the cut-off, and δn_0 the turbulence amplitude profile . Here we choose the following formula to get the value of 1 of the gradient at L , which gives us :

$$n(x, y) = n_c \left[1.25 - \frac{(1.5L_0 - x)^2}{L_0^2} \right] + \delta n_0(x) \delta n(x, y)$$

The negative values of the profiles are then shifted to zerosm to prevent unphysical event, which has the efet of making a bigger vaccum layer in the simulations. The dependancy of δn_0 will take severql form, from constant to linear, quadratic or exponentially ponderated [20], this scaling of the turbulences is done to mimic the true turbulence profile (REF), and to avoid the non natural preponderance of turbulences while working with small amplitudes. This exploration of the density profile is motivated by the fact that at the edge of the plasma, the relative amplitude of the turbulence profile is higher than in the core of the plasma. For reproductibility the parameters of the 1d simulation used to build the considered datasets are given bellow: .

Parameters range

δn_0	l_{cx} -[cm]	L -[cm]	N_x	n
$[1e^{-3}, 1]$	$[0.1, 1]$	$[7, 20]$	5000	10000



V Results

A good way to evaluate the model is to study the residuals of this latter for each parameters value of the testing set. It allows to have a quick overview of the performance model, and on the impact of parameter value on the model performances.

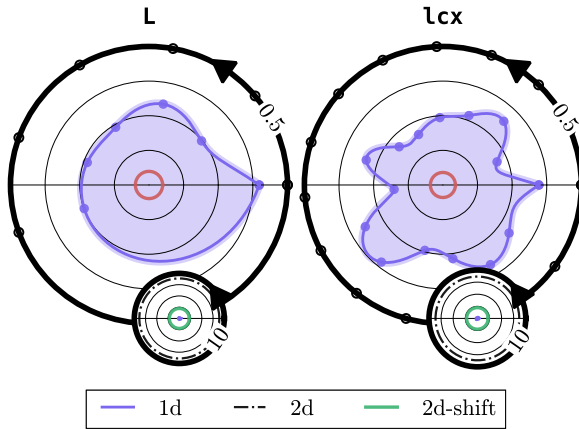


Figure 2.3: Plot of the amplitude residuals of the model for the 1D testing set in Non linear regime, the residuals are measured given a value of the studied simulation's parameter. The filled curved stands for the amplitude residuals exponentially rescaled to the real amplitude value. The red line in the center of the plot is the τ_0 mean residuals, far bellow the mean amplitude residuals. The second smaller polar shows the comparison of the residuals for several datasets : the plot of the mean amplitude residuals for the 2D datasets (black dashed curve), the amplitude residuals for the 1D datasets (blue curve in the center), and the plots of the residuals for the 2D datasets shifted to the 1D delay distribution (green curve).

From this we reach a final score of 0.94 without the moment and 0.96 with the moments on the 1d test datasets. However, with the 2d datasets the results appear to be catastrophic. The model generally predict an amplitude level one order of magnitude below or higher than the real one.

The figure 2.3 unearths quite good results regarding the 1D model prediction for the 1D testing simulation datasets, the predicted is generally of the same order of magnitude than the real one, and the residuals are quite well distributed among all the simulation parameters which is quite comforting. However, when we try to generalize the model to a higher dimension, here 2D simulations we reached very bad results with a mean amplitude residuals value of 10 for any simulations parameters. This can be explained by the fact that 1D simulations does not take into account multiple scattering effect when we reach non linear regime (see 1.6), however we can note that in non-linear regime on the 1D testing simulation datasets the model is far more performant than the analytic one. However, one can question the fact that the delay distribution is similar between the 2D case and the 1D case. Indeed, for the same 1D parameter, we can find a shift between the mean value of the delay for the 2D simulations sets and the 1D simulations set, this is due to the layer of void added around the computation domain in the 2d simulations [20], and also because the pulse is not

launched at $t = 0$. Then, if we shift the 2D simulation delay datasets to the 1D simulations delay (which is of course questionable), we reach quite a good score even in non-linear regime (this observation has been done with a flat 2D geometry, and does not take into account crucial 2D simulation parameters as the probing angle or the curved profile), the residuals obtained is the order of 2 times the value of the amplitude which is relatively good knowing the logarithmic scale of the amplitude during the training process.

However, one can ask if the study of the pulse shape with different of its characteristics can lead to better results. Indeed it will be necessary to take into account the multiple scattering effect, and the dispersive effect of the plasma. This will be the subject of the next chapter.

CHAPTER 3

2 dimensional Model

Considering a 2 dimensional model allows us to take into account several interesting effects that play a great role in the **SPR** diagnostic. Indeed, the 1D model restricted the study to delay distribution. With the CUWA 2D simulations, in addition to the delay we can study the pulse shape and its statistical properties. Furthermore, this added dimension supports the curvature $\frac{1}{R}$ study which is implied by the tokamak geometry. We can also tweak the probing wave incidence angle θ , we will study the impact of these new model's parameters on the model performances, and see if the introduction of more complexity in the model can lead to better results, with the 2d simulations datasets.

I Pulse shape Study

The goal of the pulse shape study is to find the best metrics that carry the most information as possible, in order to make our model lighter and more efficient.

1 Relative Study of Pulse Shape

For this part of the study we will limit ourselves to a simple slab geometry with normal probing, without considering any curvature and incident angle. The pulse shape can give us some information about the plasma density profile, since the pulse shape can be modified by the presence of perturbations due to multiple scattering effects and dispersive effects [see 1.6]. The dependence of the pulse shape over the background density profile will be also studied with linear, quadratic and linear modified perturbation profile. One can expect to have a much larger and randomness dependent pulse, at high turbulence amplitude due to multiple scattering. Indeed the reflected pulse will be a superposition of all scattered pulses, which should be characterized by a growing tail of the pulse distribution in delay and in width.

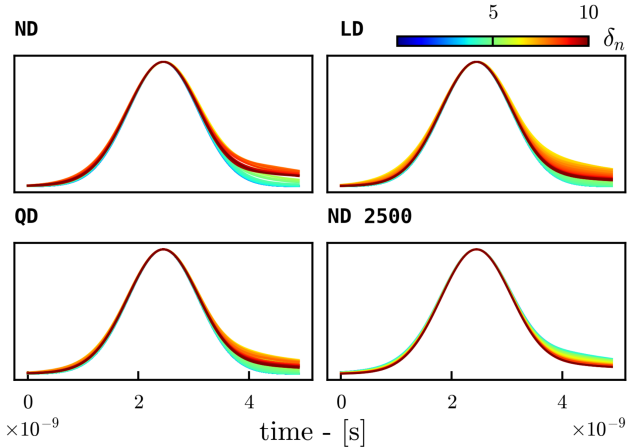


Figure 3.1: Normalized Mean of reflected pulse signal, for several density profile **ND** stands for linear density profile with a linear dependency of δn_0 over x , **LD** is a simple linear density profile with a constant turbulence amplitude, **QD** is the quadratic density profile, **ND 2500** is a 2500 samples simulations (the amplitude range is no more respected for this one due to computation cost).

For all density profile, the pulse shape is getting broader and broader for large perturbations, and the delay is getting larger and larger. This is due to the presence of multiple scattering, and dispersive effects. From this overview of the normalized mean pulse shape, we can see that a interesting metrics for our model should measured how much the mean pulse is skewed. This can be characterized by the study of the mean skewness of the pulse shape. (One other interesting parameter to highlight is the hysteresis of the normalized mean pulse(i.e the ratio of the right area over the left area of the pulse)).

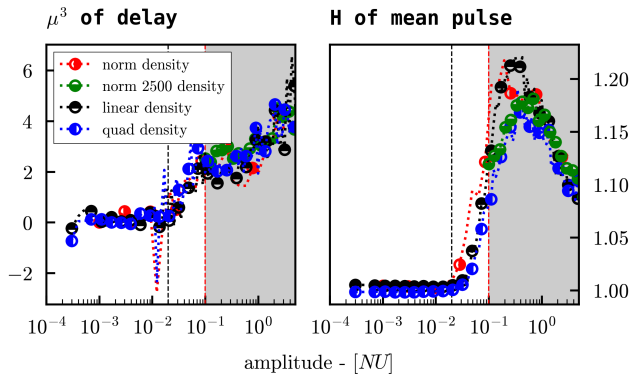


Figure 3.2: Here we computed the skewness μ^3 and the hysteresis H of the mean pulse for the previous density profiles, as intended the skewness of the pulse is increasing, the hysteresis evolution is even more pronounced. One important thing to note, is that both of the metrics are governed by the second critical density value ??, when multiple scatterings are non-negligible.

The two last metrics seems to be relevant input variables two described the relative pulse shape evolution over the amplitude level. After studying the evolution of the normalized mean pulse shape, we can study the statistical properties of the pulse shape, in order to find some relevant metrics to consider for our

model. Furthermore, it highlights that to build our Non-Linear regime dataset, we need to include in the amplitude range both critical values, because they defined important variations respectively in the delay distribution and in the pulse shape characteristics.

2 Statistical Study of Pulse Shape

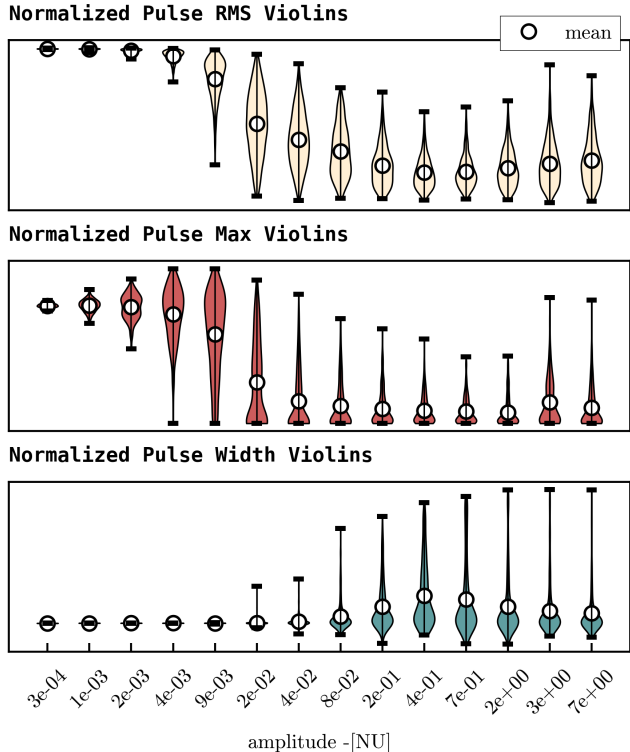


Figure 3.3: Here we plot the distribution of the pulse rms, amplitude and width for different perturbation amplitude, for the linear profile background profile **LD**. The distribution of the pulse rms and amplitude is getting broader and broader during the transition regime, this is due to randomness introduced by the perturbations, which seems to remains at large amplitudes, even if the distribution is getting quite constant. Both amplitude and rms of the pulse are highly correlated seems to catch the same dependency over the amplitude level and characterizes the transition regime between the two critical densities. The pulse width distribution study seems to be more relevant in the Non linear regime with a very smooth evolution of the standard deviation and the maximum of the pulse width, we can note that the mean of the pulse width seems to be quite constant, and do not catch enough information to be studied.

From this study several conclusions can be drawn. First the mean of the pulse amplitude seems to catch enough information for the pulse amplitude distribution characterization. Secondly the pulse standard deviation evaluation is quite redundant with the amplitude study. And finally, the pulse width study through the standard deviation of this latter can lead to interesting information, especially in full non-linear regime (after the second critical density). These conclusion have been drawn with a simple linear density profile, we tested the two others density profiles (**ND**, **QD**), and it leads to the same tendencies. The only things we found, is a shift in the delay distribution due



to the bigger vacuum layer when we use a quadratic density profile (see EQ)

3 Gaussian fitting of the pulse

One way to see the deformation of the gaussian pulse is to track the relative error of the gaussian pulse with a gaussian fit. Furthermore, it allows to study the true gaussian standard deviation, mean and amplitude. This is shown in the following figure, where we plot the relative error of the gaussian fit, and the gaussian fit

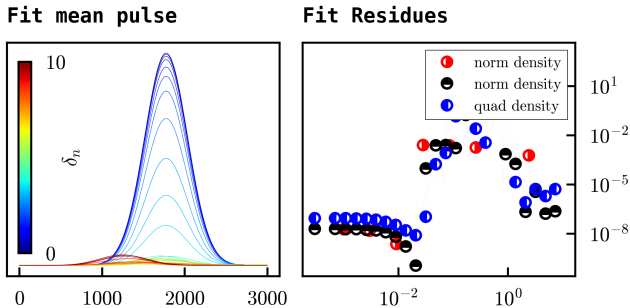


Figure 3.4: The relative error of the Gaussian fit (residuals ponderated by the size of the respective pulse amplitude) is getting large for the transition zone of the pulse shape, and seems to decline for very large turbulence. However we have to find smooth metrics to characterize the transition, and not a pseudo-random one to have better predictions in the next part. The gaussian parameters are also good candidates and are plotted in the next figure

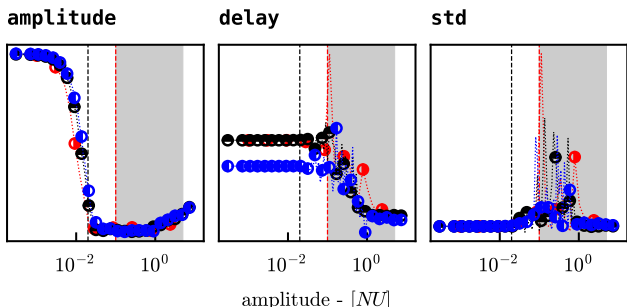


Figure 3.5: Gaussian pulse delay and standard deviation have chaotic behavior during the transition regime, this made them not relevant candidate for the next study. However let's note that the gaussian pulse amplitude, have quite a smooth behavior, but underneath a plateau during the non linear linear transition, which might not be a good option, even if at large amplitude we capture the same behavior as for the non gaussian amplitude. In a much cleaner way, indeed it's clearly increasing, this might be interesting to study the highly non linear regime.

4 Detection of scattered pulse

An other way to see the effect of non-linear regime on the probing pulse is to study the multiple scattering effect on this latter. For example we can imagine that the number of secondary spikes should be a good indicator of the non-linear regime, the amplitude of the scattered pulses should be also interesting. To do so we have to introduce a systematic method to detect all

the spikes, this has been done using the **spikefinder** library, which is a python library that allows to detect all the spikes in a signal. The following figure shows the number of spikes detected in the pulse signal, and the amplitude of the spikes.

II Datasets building

For the two dimensional datasets we select the following pulse metrics in addition to the quantilized delay distribution : mean of pulse amplitude, standard deviation of delay, mean of Hysteresis, skewness of the mean pulse, standard deviation of pulse width. In every case we begin to generate a 2d dataset based on a spectral density field. The real field is then obtained using the inverse fourier transform of the $\delta n(\mathbf{k})$ field. For each simulations we recorded the pulse signal with and without the turbulence field, and this for approximately 500 samples. The raw data is then processed online on **LEONARDO** to get the pulse metrics, and the delay distribution. This data is then saved in a SQL dataset build for this purpose and then transferred to the SPC computer for small data operations. We followed the same procedure as for the 1D dataset, with standard normalisation, and same training/testing split, with the simulation parameters as input with the previous metrics and δn_0 , τ_0 as output.

1 Gaussian spectrum of the turbulences

The gaussian spectrum is the most simple way to model the turbulence, and was used as first approximation to see if the model could integrate the dependency of the different correlation length. The parameter used for the 2D simulations with the CUWA code on **LEONARDO** are the following : θ stands for the incident angle of the probing beam, R the geometry curvature, l_{cx} the typical correlation length of the turbulence in the x direction, and l_{cy} the typical correlation length of the turbulence in the y direction. The R range is chosen to tackle flat and near TCV tokamak geometries, θ values are dependant of the R range and cannot be too high, indeed if we consider a high curvature the incident angle cannot be too high, because the probing beam will not be able to reach the cut-off layer, or will be reflected not in the direction of the antenna, this is why we limited ourselves to 10 degrees, with $R = 0.2$ m. In the gaussian case, the power spectrum of the turbulence is given by the following formula :

$$\delta n(\mathbf{k}) = \delta n_0 \exp\left(-\frac{(k_x l_{cx} k_y l_{cy})^2}{8} + i\Phi(\mathbf{k})\right)$$

This formula will be used to create the first part of the dataset with defined correlation lengths. But one could argue that the power spectrum of **TEM** instabilities is not gaussian.

2 Power Spectrum of the turbulences

Indeed the power spectrum of the turbulences is a more realistic approach to the turbulence profile, (give the detail for each literature measurements of the knee power spectrum). Then explain why the power spectrum is much more complicated to have a continuous one. Then introduce the formula of the power spectrum used [cite], and the different parameters used .

$$\langle \delta n^2 \rangle = \frac{1}{1 + |\frac{k_x}{W_x}|^\gamma + |\frac{k_y - k_y^*}{W_y}|^\beta}$$

With W_x the x spectral width, W_y the y spectral width k_y^* the injection driving scale of the instabilities



[CITE]. Note that all the parameter are normalized by ρ_s the ion gyro-radius. This formula has the advantage to not be separable in x and y , which is the case in ... [cite]

a) COrrelation length dependancy study

As it is not determined by the power spectrum formula we have to shift to measured lc as an input for the model. This is why its convenient to have a relationship between all the parameters and the correlation length. The expression of $l_{cx, cy}$ can be found using the **CCF** on many field sample (s).

$$r_{xx}(\tau) = \frac{\sum_s (\tilde{\delta n}_s(x + \tau, y)) (\tilde{\delta n}_s(x, y))}{\sum_s (\tilde{\delta n}_s(x, y))^2}$$

With $\tilde{\delta n}_s(x, y) = \delta n_s(x, y) - \bar{\delta n}_s(y)$. The Wiener-Khinchin theorem [CITE] brings an other method to compute the correlation length without the need of having many samples indeed supposing k_y constant for the integration we have for the x correlation length :

$$r_{xx}(\tau) = \int_{-\infty}^{\infty} < \delta n(k_x, k_y)^2 > e^{2\pi k_x \tau} dk_x$$

With r_{xx} the autocorellation function. The correlation length is then defined when the r_{xx} reaches the e^{-1} level, then developing the expression of the power spectrum, we have :

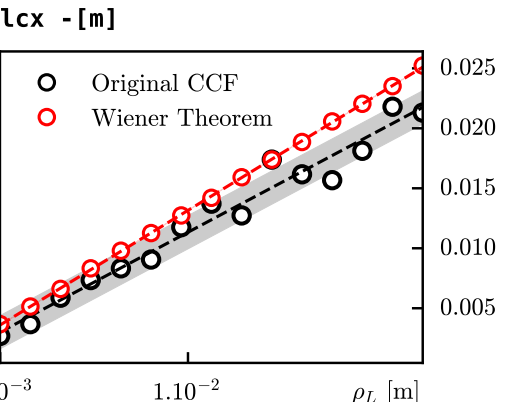
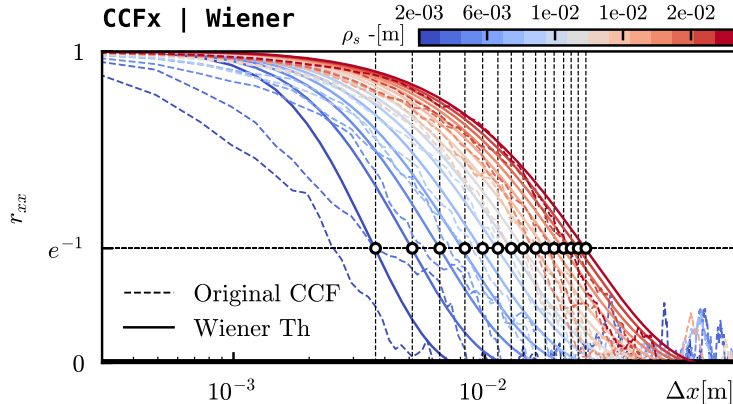


Figure 3.6: On the left plot the r_{xx} computed with the **CCF** and Wiener Theorem, for several ρ_s . On the right the linear fit between the correlation and the ion gyro-radius. The same study has been done for the y correlation length dependancy study.

The correlation length fit of the Wiener theorem appears to have the smallest residuals, and leads to the same results as the **CCF** method, without computing too many samples. We can then obtain the following formula for the correlation lengths which should leads to the same turbulence structures as the gaussian spectrum (see fig: 3.7) :

$$\begin{cases} l_{cx} = (1.19 \pm 0.02)\rho_s + (0.0012 \pm 0.0001) \\ l_{cy} = (1.35 \pm 0.03)\rho_s + (0.0015 \pm 0.0001) \end{cases}$$

We can then use these formula to compute the correlation length for the 2D datasets which will be input parameters for our model, and then use the power spectrum formula to compute the $\delta n(\mathbf{k})$ field. The pa-

$$r_{xx}(\tau) = \int_{-\infty}^{\infty} \frac{1}{1 + |\frac{k_x}{W_x}|^\gamma + |\frac{k_y - k_y^*}{W_y}|^\beta} e^{2\pi i k_x \tau} dk_x \quad (3.1)$$

$$= \int_{-\infty}^{\infty} \frac{e^{2\pi i k_x \tau}}{1 + |\frac{k_x}{W_x C^{1/\gamma}}|^\gamma} dk_x \quad (3.2)$$

From this we can see that the autocorrelation function has a spiked shape, whose width is linearly proportional to : $\frac{1}{W_x C^{1/\gamma}}$ with $C = 1 + |\frac{k_y - k_y^*}{W_y}|^\beta$, the same reasoning can be done for the y correlation length, with the same width dependancy, this leads to the following dependancy :

$$l_{cx} \propto \left(\frac{1}{W_x C^{1/\gamma}} \right), l_{cy} \propto \left(\frac{1}{W_y Z^{1/\beta}} \right)$$

With $Z = 1 + |\frac{k_x}{W_x}|^\gamma$. For large scale turbulences like TEM, the spectral width is greater than the wave number since it's known to be large scale phenomena, this leads to $C \approx 1$ and $Z \approx 1$. We then have :

$$l_{cx} \propto \frac{1}{W_x} \propto \rho_s, l_{cy} \propto \frac{1}{W_y} \propto \rho_s$$

Then we numerically computed the correlation length using true **CCF** and Wiener-theorem to determine the proportionality constant for both, x and y , cases. Thanks to that we can keep the correlation length as an input for the model, and not the spectral width, which is more difficult to measure.

parameters used for the 2D simulations with the CUWA code on **LEONARDO** are the following :

Parameters range				
δn_0	L -[cm]	ρ_s -[m]	θ -[°]	R -[m]
$[1e^{-3}, 1]$	$[5 - 18]$	$[2e^{-3}, 2e^{-2}]$	$[0-10]$	$[0.2, 5]$

Table 3.2: 2D simulation parameters range based on Power spectrum, the value of ρ_s are choosen to be included in the range of the gaussian dataset values of l_{cx} and l_{cy}

Note that for generating the $\langle \delta n \rangle^2$ field we took, $D = 6.3e^{-3}(\frac{\rho}{L})^2$, $W_x = \frac{3.71}{\rho_s}$, $W_y = \frac{4}{\rho_s}$, $\beta = 2.88$, $\gamma = 3.14$, $k_y^* = \frac{0.1}{\rho_s}$. The l_{cx} and l_{cy} 'calibration' (fig: 3.6) was done using this values used in [CITE]

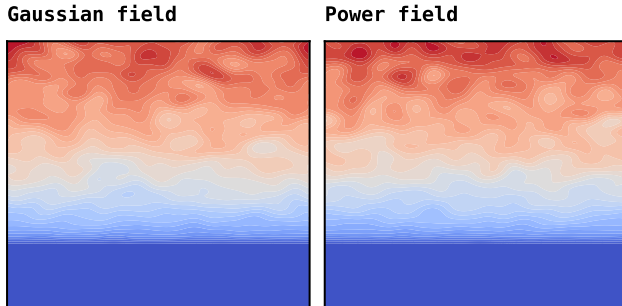


Figure 3.7: Comparaison of both structure with $\rho_s = 8e^{-3}$ of the turbulence field (we used the same corelation lengths in the gaussian spectrum). The selected plotting zone in a (3cm x 10cm) rectangle including the cut-off layer and the vaccum layer

In fig:3.7 we can denote the same structure of the turbulence field for both spectral approach which menas that our first gaussian approximation is quite relevant and should help our model to generalize his prediction to both cases.

3 data scanning

For the first part of the training to have homogeneous data distribution we chose data points on a defined grid, then to refined the model we used some random uniformly sample (logarithmicly for δn_0) data points in the range of the study. To see if the reached distribution is quite homogeneous for the training we can plot the distribution of the data points in the parameter space, and see if the data points are well distributed. This is done in the following figure.

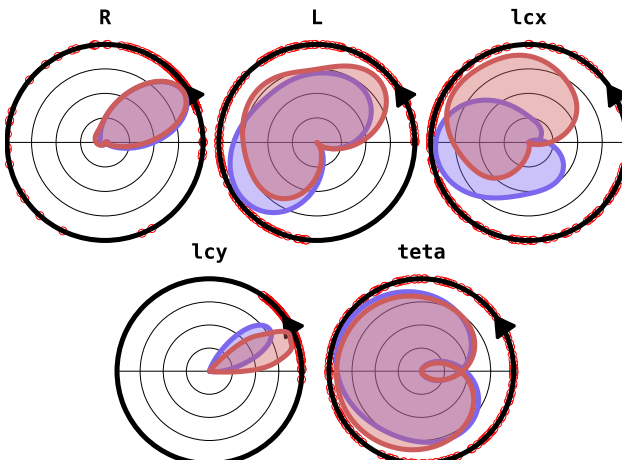


Figure 3.8: Polar distributions of the params, the circle corresponds to the parameter range (described in table 3.2 and table ??), and the radial value to the parameter distribution value. In blue the power spectrum datasets and in red the gaussian spectrum datasets.

The fig: shows that the data points are quite well distributed in the parameter space, the that we can note is that the R distribution is concentrated near 0, because we choose to plot the curvature $\frac{1}{R}$ distribution wheter than the true radius doistribution (indeed to account for flat geometries we introduced $R = 1000$ value in the datasets, which should have broken the normalization process in the datasets).The last thing to highlight is that the l_{cy} distribution is also unevenly reparted, since we also introuced high value of l_{cy} in the datasets to mimic the 1 dimensional case. We finally end up with more than 2000 datapoints with 500 samples for each points. Before the training, we followed the same procedure as for the 1D datasets, with standart normalisation, and same training/testing split, with the simulation parameters as input with the previous metrics and δn_0 , τ_0 as output.

III Results

The model was trained on the 2D datasets, with the same structure as the 1D model (which was found quite robust for tackling non linearities)the same hyperparameters are used for this study (see table ??). The only thing changing is the number of input data variable, which complexify our model.

1 Global performance

The model reached a R^2 score of 0.92 for the gaussian testing set, and 0.89 for the power spectrum testing set. Which are quite reasonable results even for the logarithmic dependancy of δn_0 . For comparison, a deep neural network has been trained in parallel of our model with the same dataset with 5 layers of respectively (256,128,64,32,2) neurons in each layer with sigmoid activation, this model begins to be quiet complex and reach a poor R^2 score of 0.3, which is far behind our performances. To have a better overviwe we can follow the sampe principle used in the figure ??, comparing the residuals of the model for each parameter value of the testing set. This is done in the following figure.

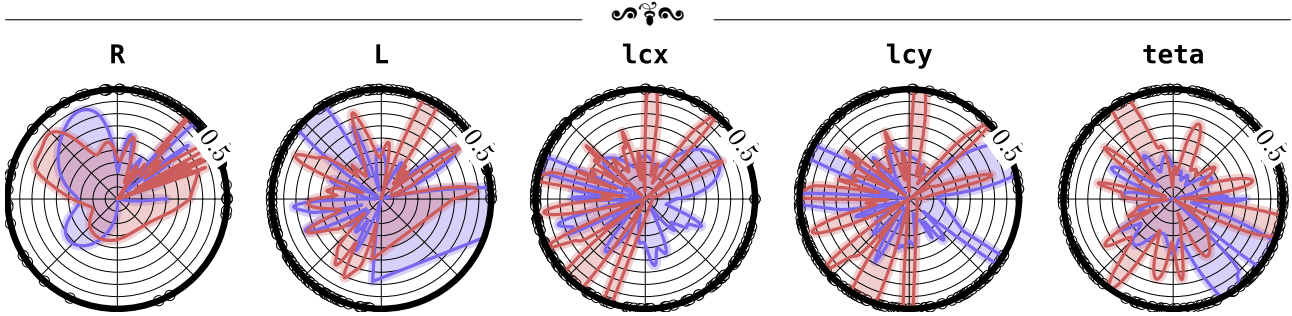


Figure 3.9: Here we plot the mean residuals for every value of every parameter, in blue filled we got the residuals for the gaussian datasets, and in red the residuals for the power spectrum datasets. One remarkable thing is that the model is far more better than the 1D model in both datasets, which is quite comforting. Indeed we reach a mean residual of 0.25, ten times smaller than the 1D model apply to the 2D-shifted datasets. An other interesting thing is that the residuals are quite well distributed among all the simulation parameters, however one can note that the residual over the R values are quite focused on the lower values, but this is simply a consequence of the $\frac{1}{R}$ transform. An other interesting results is that the θ parameter residuals seems higher for high value of θ which seems reasonable, since these cases are much more difficult to handle. Regarding the difference between the two datasets the residuals have globally the same mean value, which is comforting, and leads to quite good generalization of the model.

2 Comparison of the prediction with other models

For the previous study the datasets contained several parameters that implied a 2D geometry. However, if we wanna compare the model with the 1D model, and the analytical one we have to build a final comparison datasets. To have clear results we will fix the l_{cy} , R , θ , L , l_{cx} parameters to the same value for the 1D and 2D model, then we will see if our model is able to handle the simple 1D case with the study of the dependancy of predicted δn_0 over true δn_0 , which is a more general way to study $\text{rms}(\tau)$ over δn_0 . An other interesting results to have as comparison is the fact that for the 1D analytic model (eq ??) we have the following equation $\langle \tau \rangle = \tau_0$.

a) Mean delay study

In non linear regime the previous assumption is broken, and our model should be able to handle this case, to see this effect we can study the dependancy of τ_0 over δn_0 . Indeed, for the delay shift to be 0, we should have the same probability to make a shift of δx of the cut-off layer in the left or in the right direction which is not the case in the non-linear regime, indeed we have a higher probability to have a negative shift than a positive shift, indeed let's consider a given n_c and δx value. We will consider a 1d model with a density variation PDF that does not take into account the spatial correlation length, this leads to the following :

$$p(\delta n, x) = \frac{1}{\sqrt{2\pi\sigma^2}} e^{-\frac{\delta n^2}{2\sigma^2}},$$

With $\sigma \propto \delta n_0$ We are looking for the first-hitting-position, this is a sub-branch of the survival stochastic analysis, the probability of survival $S(x)$ (i.e the probability that the density does not reach the δn_c value before x) is always given for constant δn_c relative to x or in our case the critical density variation is $\delta n_c = n_c \frac{L-x}{\sigma}$. The goal is to show that the probability of first hitting position is decreasing with x . This study implies to take into account the correlation length of the instabilities field, indeed if we do not, the survival probability will be just equal to 0. For simplicity we will discretized the interval of study $[0, x]$ with

$\left\lfloor \frac{x}{l_{cx}} \right\rfloor$ points (here the argument is that every points in each interval of length l_{cx} has the same probability of survival which is equivalent to the step approximation, the probability of having a value smaller than δn_c at a specific point i is given by the following formula :

$$\begin{aligned} P(\delta n_c, ia) &= \int_{-\infty}^{\delta n_c} p(\delta n, ia) d\delta n \\ &= \frac{1}{2} \left(1 + \text{erf} \left(\frac{\delta n_c(ia)}{\sigma} \right) \right) \end{aligned}$$

The survival probability at point $x = ia$ is then given by the following formula :

$$S(ia) = \prod_{j=0}^i P(\delta n_c, j * a)$$

The probability that the first hitting position is at $x = ia$ is then given by $F(ia) = S(ia)P(ia)$. The goal of this study is to show that $F(x)$ maximum is located before the original cut-off position. To show this we computed numerically the value of the value of $S(ia)$. With this computation we find an interesting approximation of the survival function (see ??) in this gaussian (shifted) process has been numerically find to be :

$$S(x) \approx \frac{1}{2} + \frac{1}{2} \text{erf} \left(\frac{L - x - a(l_{cx}, L, \sigma)}{b(l_{cx}, L, \sigma)} \right) \quad (3.3)$$

With $a(l_{cx}, L, \sigma)$ the characteristic shift and $b(l_{cx}, L, \sigma)$ a characteristic width, This approximation is the probability to remains bellow the critical value at a position $x - a(l_{cx}, L, \sigma)$ with a modified distribution of instabilities amplitude $\mathcal{N}(0, b(l_{cx}, L, \sigma))$. We can note that this results is really close from the survival function of a brownian process considering an absorption point x_c the first hitting time method used in this kind of problem were not transposed here due to the linear shifted of the gaussian distribution which was very difficult to



handle, because we need to consider a moving absorption point to make the parallelism.

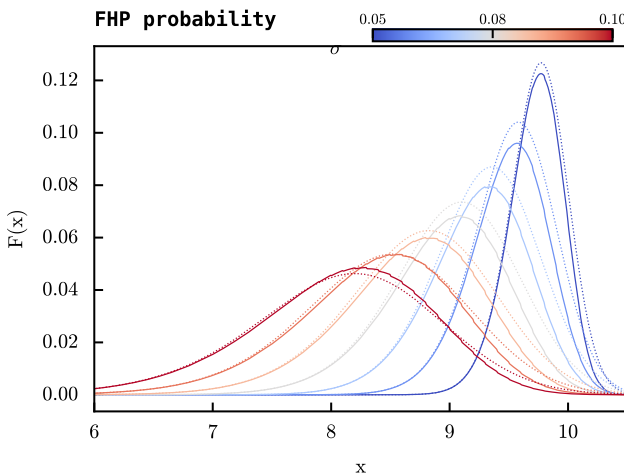


Figure 3.10: Here we plot the numerical calculation of $F(x)$ the First timeHitting probability (**FHP**) for numerous σ in plain line and the approximated formula (3.3) in dotted line. For this simulation we used $L = 10\text{cm}$ and $l_{cx} = 0.1\text{cm}$, and for the approximated formula we used $a = 2.1\sigma^{1.5}L$ and $b = .36\sigma^{0.8}L$, we did not study the dependancy over l_{cx} but this one is clearly in the power and the coefficient of a and b .

One can remarks that the **FHP** is shifted to the values before L while σ is increasing, which explains the radial external shift of the cut-off with the increasing of the amplitude of turbulences, indeed we can assume a linear dependacy between σ and δn_0 . This shift will results in a difference between $\langle \tau \rangle$ and τ_0 . With τ_0 remaining constant and $\langle \tau \rangle$ decreasing. We already know that the linear model is not able to have this precision, what about the new ones.

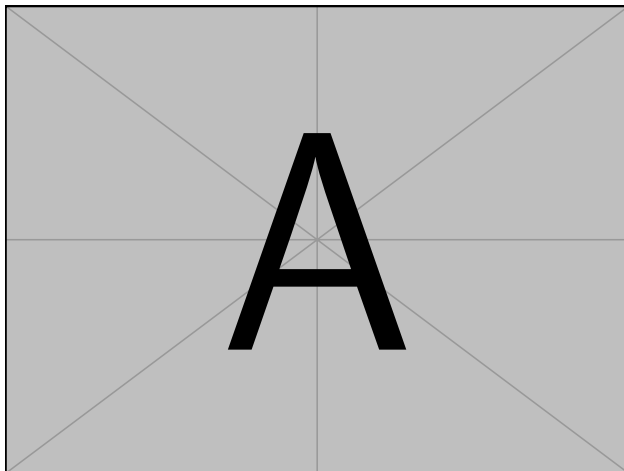


Figure 3.11: Here we plots the linear and the 1d, 2d model prediction for τ_0 over the $\langle \tau \rangle$.

Here we can see that the 1d model and the 2d model build on the same architecture are able to predict a constant τ_0 independantly of the changing delay distribution. This was intended since the model are trained on constant τ_0 just depending on L, R, θ .

b) Amplitude prediction study

The first thing we did is comparing the efficiency of all the modle we build with the $(\delta n_0, \delta n_0^{\text{pred}})$ comparison. Which is, taking into account the results of the residuals be much more better for our last model than for the others. The more the points are dispersed from the identity the worse is the model, several conclusion on the training efficiencu can also be studied from the study of the residuals of this predction.

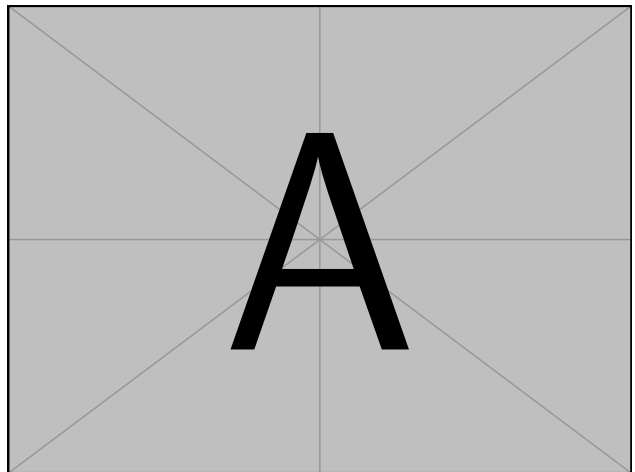


Figure 3.12: Here we plots the linear and the 1d, 2d model prediction for τ_0 over the $\langle \tau \rangle$.

c) standard deviodation of delay

As explained with the 1.6 the rms of the delay distribution should decrease at high amplitude from δn_{c1} . Thi decreasing is not tackled with the linear model (the next order of the step model devlopment have to be studies), at least not correctly (see the third order devlopment of the linear model). The previous model should present better results considering the residuals of the predictions.

3 Results on experimental datasets

A demonstration of our final model was done on one expeimental dataset acquired from the TCV diagnostics. To have coherent results we had to shift the experimental datasets distribution of delay to the training one. This constant shift is due to the geometry of the probing method, with a different void layer. This process will be necessary for the next studies, one solution is too have a consistant dataset with the same range of data than our training datasets (see table PUT), or to train the model on an other dataset specific to the geometry and diagnostic method used (see the code of the model HERE),

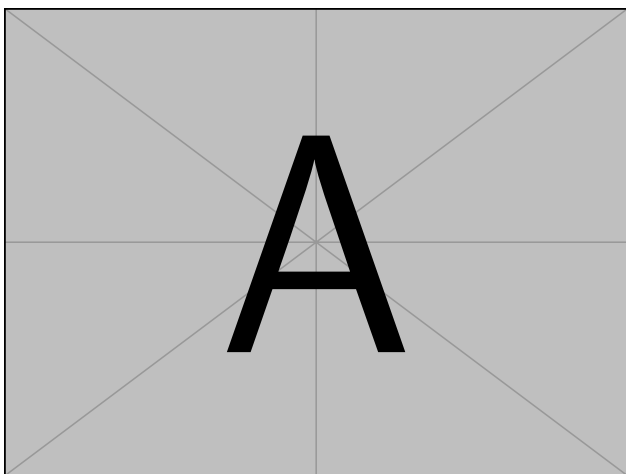


Figure 3.13: Here we plots the linear and the 1d, 2d model prediction for τ_0 over the $\langle \tau \rangle$.

CHAPTER 4

Conclusion and Discussion

In this report we first detailed the origin of **TEM** mode and how they can induce a uncontrolled radial transport, causing trouble for plasma confinement. We then used a 1d model (proposed by Krutkin) to have

first insights of the turbulence regime, and to what extent the linear model can be relevant. We then move on the analysis on a 1 dimensional dataset, checking if the non linear regime could be tackled by the model structure. A more general 2d model was then proposed with a better handling of non linear effect emerging from this added dimension, this model includes more metrics that have been cautiously chosen to have the best overview of the phenomena at stake. Finally, The model predictions have been tested on several aspect of the problem through the shifted cut-off handling to the decreasing of the rms of the delay distribution. This leads to significantly good results, which were not reached before for turbulence characterizations. One can note that our model is built on the assumption that we have sufficient insight on the turbulences characteristics such as the correlation lengths that can be determined through other diagnostic methods (Doppler Reflectometry Method and Thomson Scattering). If the future users of this model do not have this insights one can build a reduced model dropping every metrics they do not have. We should highlight that the delay distribution and the pulse characteristic (at least the standard deviation of the delay distribution)

CHAPTER 5

ACKNOWLEDGMENTS

Bibliography

- ¹T. J. Dolan, “Plasma heating and current drive”, in *Magnetic fusion technology*, edited by T. J. Dolan (Springer London, London, 2013), pp. 175–232.
- ²A. Piel, *Plasma physics: an introduction to laboratory, space, and fusion plasmas*, Graduate Texts in Physics (Springer International Publishing, 2018).
- ³L. Qi, “Energy transfer of trapped electron turbulence in tokamak fusion plasmas”, *Scientific reports* **12**, 5042 (2022).
- ⁴Y. Xiao and Z. Lin, “Turbulent transport of trapped-electron modes in collisionless plasmas”, *Phys. Rev. Lett.* **103**, 085004 (2009).
- ⁵T. Xie, Y. Z. Zhang, S. M. Mahajan, F. Wu, H. He, and Z. Y. Liu, “The two-dimensional kinetic ballooning theory for trapped electron mode in tokamak”, *Physics of Plasmas* **26**, 022503 (2019).
- ⁶W. Horton, “Drift waves and transport”, *Rev. Mod. Phys.* **71**, 735–778 (1999).
- ⁷O. Krutkin, “Theoretical analysis and full-wave simulations combined in the development of the synthetic doppler reflectometry diagnostics for tokamaks”, PhD thesis (June 2020).
- ⁸M. A. Mitsuru Kikuchi, *Frontiers in fusion research ii, introduction to modern tokamak physics*, edited by Springer (Springer, Naka, Ibaraki, Japan, Setagaya, Tokyo, Japan, 2015).
- ⁹K. Miyamoto, *Plasma physics and controlled nuclear fusion* (Jan. 2004).
- ¹⁰V. Rozhansky, *Plasma theory an advanced guide for graduate students* (Springer, St. Petersburg, Russia, 2023).
- ¹¹S. C. Prager, A. K. Sen, and T. C. Marshall, “Dissipative trapped-electron instability in cylindrical geometry”, *Phys. Rev. Lett.* **33**, 692–695 (1974).
- ¹²A. Hasegawa and M. Wakatani, “Self-organization of electrostatic turbulence in a cylindrical plasma”, *Phys. Rev. Lett.* **59**, 1581–1584 (1987).
- ¹³M. Wakatani and A. Hasegawa, “A collisional drift wave description of plasma edge turbulence”, *The Physics of Fluids* **27**, 611–618 (1984).
- ¹⁴B. Kadomtsev and O. Pogutse, “Trapped particles in toroidal magnetic systems”, *Nuclear Fusion* **11**, 67 (1971).
- ¹⁵A. Hasegawa and K. Mima, “Pseudo-three-dimensional turbulence in magnetized nonuniform plasma”, *The Physics of Fluids* **21**, 87–92 (1978).
- ¹⁶P. H. Diamond, *Theory of magnetically confined plasma*, <https://courses.physics.ucsd.edu/2021/Spring/physics218c/handouts.html>, 2021.
- ¹⁷Z. Lin, Y. Xiao, W. Deng, I. Holod, C. Kamath, S. Klasky, Z. Wang, and H. Zhang, “Size scaling and nondiffusive features of electron heat transport in multi-scale turbulence”,
- ¹⁸G. Falchetto, J. Vaclavik, M. Maccio, S. Brunner, and L. Villard, “Applicability of the ballooning transform to trapped ion modes”, *Physics of Plasmas* **7**, 1196 (2000).
- ¹⁹P. Aleynikov and N. B. Marushchenko, “3d full-wave computation of rf modes in magnetised plasmas”, *Computer Physics Communications* **241**, 40–47 (2019).
- ²⁰O. Krutkin, S. Brunner, and S. Coda, “A method for density fluctuation measurements using pulse reflectometry”, *Nuclear Fusion* **63**, 10.1088/1741-4326/acd5e0 (2023).
- ²¹J. R. Ruiz, F. I. Parra, V. H. Hall-Chen, N. Christen, M. Barnes, J. Candy, J. Garcia, C. Giroud, W. Guttenfelder, J. C. Hillesheim, C. Holland, N. T. Howard, Y. Ren, A. E. White, and J. contributors, “Interpreting radial correlation doppler reflectometry using gyrokinetic simulations”, *Plasma Physics and Controlled Fusion* **64**, 055019 (2022).
- ²²H. Biglari, P. H. Diamond, and P. W. Terry, “Influence of sheared poloidal rotation on edge turbulence”, *Physics of Fluids B: Plasma Physics* **2**, 1–4 (1990).
- ²³L. Vermare, P. Hennequin, Ö. D. Gürcan, C. Bourdelle, F. Clairet, X. Garbet, R. Sabot, and the Tore Supra Team, “Impact of collisionality on fluctuation characteristics of micro-turbulence”, *Physics of Plasmas* **18**, 012306 (2011).
- ²⁴J. W. Connor, R. J. Hastie, and J. B. Taylor, “Shear, periodicity, and plasma ballooning modes”, *Phys. Rev. Lett.* **40**, 396–399 (1978).

-
- ²⁵P. Molina Cabrera, S. Coda, L. Porte, A. Smolders, and T. Team, “V-band nanosecond-scale pulse reflectometer diagnostic in the tcv tokamak”, *Review of Scientific Instruments* **90**, 123501 (2019).